Structure of 6-hydroxymethyl-7,8-dihydropterin pyrophosphokinase–dihydropteroate synthase from *Plasmodium vivax* sheds light on drug resistance

Received for publication, June 27, 2018, and in revised form, August 8, 2018 Published, Papers in Press, August 13, 2018, DOI 10.1074/jbc.RA118.004558

Manickam Yogavel[‡1], Joanne E. Nettleship[§¶], Akansha Sharma[‡], Karl Harlos[§], Abhishek Jamwal[‡], Rini Chaturvedi[‡], Manmohan Sharma[‡], Vitul Jain[§], Jyoti Chhibber-Goel[‡], and Amit Sharma[‡]

From the [‡]Molecular Medicine–Structural Parasitology Group, International Centre for Genetic Engineering and Biotechnology, New Delhi 110067, India, the [§]Division of Structural Biology, Wellcome Centre for Human Genetics, University of Oxford, Oxford OX3 7BN, United Kingdom, and the [¶]Oxford Protein Production Facility, United Kingdom Research Complex at Harwell, Rutherford Appleton Laboratory, Oxford OX11 0FA, United Kingdom

Edited by Norma M. Allewell

The genomes of the malaria-causing *Plasmodium* parasites encode a protein fused of 6-hydroxymethyl-7,8-dihydropterin pyrophosphokinase (HPPK) and dihydropteroate synthase (DHPS) domains that catalyze sequential reactions in the folate biosynthetic pathway. Whereas higher organisms derive folate from their diet and lack the enzymes for its synthesis, most eubacteria and a number of lower eukaryotes including malaria parasites synthesize tetrahydrofolate via DHPS. *Plasmodium falciparum* (*Pf*) and *Plasmodium vivax* (*Pv*) HPPK–DHPSs are currently targets of drugs like sulfadoxine (SDX). The SDX effectiveness as an antimalarial drug is increasingly diminished by the rise and spread of drug-resistant mutations. Here, we present the crystal structure of *Pv*HPPK–DHPS in complex with four substrates/analogs, revealing the bifunctional *Pv*HPPK–DHPS architecture in an unprecedented state of enzymatic activation. SDX's effect on HPPK–DHPS is due to 4-amino benzoic acid (*p*ABA) mimicry, and the *Pv*HPPK–DHPS structure sheds light on the SDX-binding cavity, as well as on mutations that effect SDX potency. We mapped five dominant drug resistance mutations in *Pv*HPPK–DHPS: S382A, A383G, K512E/D, A553G, and V585A, most of which occur individually or in clusters proximal to the *p*ABA-binding site. We found that these resistance mutations subtly alter the intricate enzyme/*p*ABA/SDX interactions such that DHPS affinity for *p*ABA is diminished only moderately, but its affinity for SDX is changed substantially. In conclusion, the *Pv*HPPK–DHPS structure rationalizes and unravels the structural bases for SDX resistance mutations and highlights architectural features in HPPK–DHPSs from malaria parasites that can form the basis for developing next-generation anti-folate agents to combat malaria parasites.

Malaria remains a central cause of morbidity and mortality in humans. The malaria parasites *Plasmodium falciparum* (*Pf*)[2] and *Plasmodium vivax* (*Pv*) infect >400 million people and result in ~0.3 to ~0.4 million annual deaths worldwide (1). Malaria remains a constant public health threat because of the emergence of drug-resistant strains across endemic regions (2). Despite increased drug resistance, several anti-malarial drugs are still used clinically for the treatment of malaria infection (3). Therefore, the world health community needs to continually discover both new drug targets and novel chemical scaffolds. Tetrahydrofolate is an essential cofactor that is vital for metabolic reactions involving one-carbon transfer (4). Most notably, it is required for the synthesis of nucleic acid precursors like purines and thymidine and for methionine, glycine, and pantothenate (5). Higher organisms derive folate from their diet and lack the necessary enzymes for folate synthesis, but almost all eubacteria and a number of lower eukaryotes including malaria parasites synthesize tetrahydrofolate (5–7). The malaria parasite genomes encode fused 6-hydroxymethyl-7,8-dihydropterin pyrophosphokinase (HPPK) and dihydropteroate synthase (DHPS) domains (Fig. 1*A*) that perform sequential reactions wherein HPPK catalyzes transfer of pyrophosphate from ATP to 6-hydroxymethyl-7,8-dihydropterin (DHP) resulting in 6-hydroxymethyl-7,8-dihydropterin-pyrophosphate (DHPPP) (8, 9). Subsequently, DHPS acts as a crucial convergence point in the folate pathway and catalyzes the condensation of 4-aminobenzoic acid (*p*ABA) and DHPPP to form the intermediate 7,8-dihydropteroate (Fig. 1*B*) (10). 7,8-Dihydropteroate is then fed into the folate synthesis path-

This work was supported by grant (EMR/2016/004898) from Department of Science and Technology (DST), Ministry of Science and Technology, Government of India. This work was also supported in part by a travel grant from the Indo-French Centre for the Promotion of Advanced Research (IFCPAR/CEFIPRA) (to M. Y. and M. S.), Core Grant Award 090532/Z/09/Z from the Wellcome Centre for Human Genetics (to K. H.), and a J.C. Bose fellowship from DST, Ministry of Science and Technology, Government of India (to Am. S.). The authors declare that they have no conflicts of interest with the contents of this article.

The atomic coordinates and structure factors (code 5Z79) have been deposited in the Protein Data Bank (http://wwpdb.org/).

[1] To whom correspondence should be addressed: Structural Parasitology Group, International Centre for Genetic Engineering and Biotechnology, Aruna Asaf Ali Marg, New Delhi 110067, India. E-mail: myogavel@gmail.com.

[2] The abbreviations used are: *Pf*, *P. falciparum*; *Pv*, *P. vivax*; HPPK, 6-hydroxymethyl-7,8-dihydropterin pyrophosphokinase; DHPS, dihydropteroate synthase; RMSD, root mean square deviation; SDX, sulfadoxine; *p*ABA, 4-amino benzoic acid; DHP, 6-hydroxymethyl-7,8-dihydropterin; DHPPP, 6-hydroxymethyl-7,8-dihydropterin-pyrophosphate; SP, SDX with pyrimethamine; ASU, asymmetric unit; PtPP, 6-hydroxymethyl pterindiphosphate; AMPCPP, adenosine 5′-(α,β-methylene)-diphosphate; MR, molecular replacement; TIM, triosephosphate isomerase; PDB, Protein Data Bank.

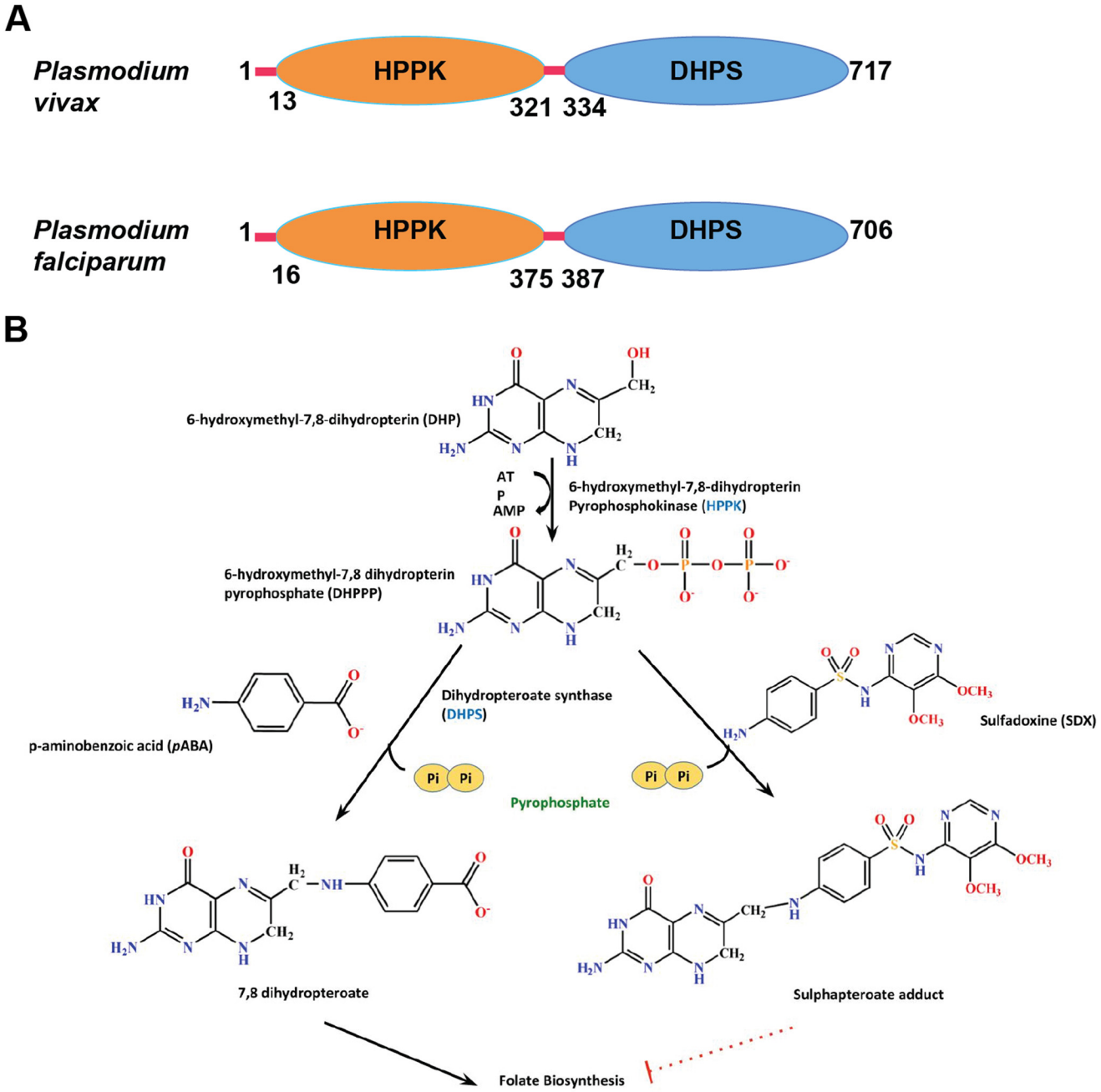

Figure 1. Structure and function of *Pv*HPPK–DHPS. *A*, the domain architecture of *Pv* and *Pf* HPPK–DHPSs (717 and 706 residues, respectively) with marked domain boundaries of HPPK and DHPS in *orange* and *blue*, respectively. The *red lines* are regions that fall outside annotated domain boundaries. *B*, HPPK domain catalyzes the transfer of pyrophosphate from ATP to DHP, resulting in the product DHPPP. DHPPP is then converted to 7,8-dihydropteroate by DHPS using *p*ABA and DHPPP. SDX inhibits DHPS via mimicry of *p*ABA where it results in formation of an adduct that is deleterious to the downstream folate synthesis pathway. The *dotted red line* indicates termination of the pathway.

way where it is converted to 7,8-dihydrofolate by the enzyme dihydrofolate synthase and subsequently to tetrahydrofolate by the enzyme dihydrofolate reductase (Fig. 1*B*). The folate pathway is therefore an ideal target for anti-infectives and has been utilized for many decades (11).

Sulfonamides target a key enzyme in folate biosynthesis pathway viz. DHPS (12). The aryl amine moiety of sulfa drugs forms a dihydropteroate-like product with DHPPP that is impotent toward undergoing subsequent dihydrofolate synthesis (13, 14). Sulfa drugs have remained important clinical agents since they were first discovered in the 1930s (15), but their efficacy has been severely impacted by drug resistance that began to emerge shortly after they were first introduced (16, 17). Despite increased resistance, sulfodaxine (SDX) is still used in combination with pyrimethamine (SP) to treat malaria (18, 19). Pyrimethamine inhibits the enzyme dihydrofolate reductase in the folate biosynthesis pathway, whereas SDX stalls DHPS activity; because of their synergistic effect, these two drugs (SP) are more effective in combination than either drug used alone (18, 19). SP is used to treat chloroquine-resistant *Pf* malaria and is the only drug combination recommended by World Health Organization for intermittent preventive treat-

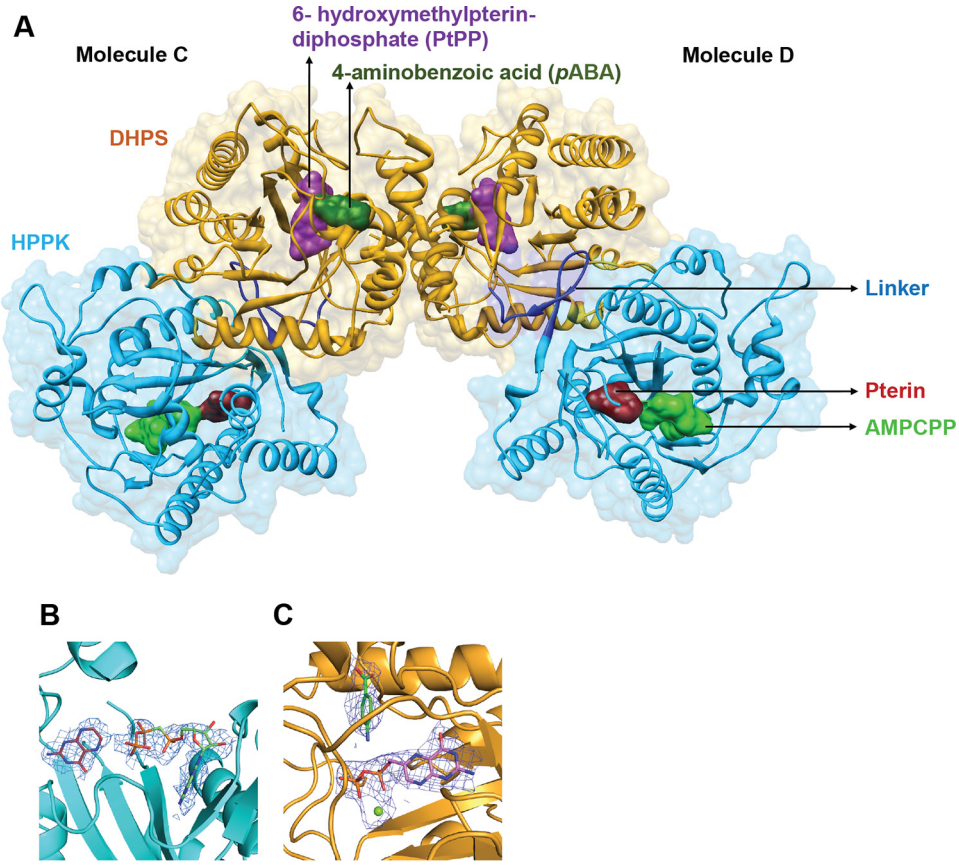

Figure 2. Crystal structure of *Pv*HPPK–DHPS. *A*, dimeric *Pv*HPPK–DHPS where bound substrate/analogs in both HPPK and DHPS domains are shown as molecular surfaces. HPPK (*cyan*), DHPS (*yellow*), and the linker regions (*blue*) are marked. The bound substrates/analogs of pterin (*maroon*), AMPCPP (*light green*), PtPP (*purple*), *p*ABA (*green*), and Mg^{2+} ion (*lime green*) are shown as *sticks* and *spheres*. *B* and *C*, the simulated annealing composite omit map contoured at 2σ levels for the bound ligands where ligands and bound Mg^{2+} ion are shown as *sticks* and *spheres*, respectively.

ment of infants as an additional malaria control in high transmission areas of sub-Saharan Africa (19–22). Increasing resistance toward SDX is therefore alarming and calls for the development of a new generation of anti-folates that are less susceptible to resistance generation but that retain the enzymatic target of DHPS.

Here, we present the crystal structure of *Pv*HPPK–DHPS in complex with its four substrates/analogs. The structure contains residues from 1 to 717, is dimeric, and reveals the juxtaposition of both HPPK and DHPS domains that are connected by a linker segment. We have mapped the conserved *p*ABA-binding residues and sites of vital mutations that tune the specificity and affinity of *p*ABA, as well as the drug SDX. This work will enhance our understanding of molecular mechanisms used by *Pv*HPPK–DHPS to develop anti-folate drug resistance and provides a new focus for development of novel anti-malarial agents.

Results

Crystal structure of PvHPPK–DHPS

Plasmodium parasite genomes encode fused genes for HPPK and DHPS. We expressed recombinant full-length *Pv*HPPK–DHPS consisting of 717 residues and crystallized it ($P2_1$ system with six molecules in asymmetric unit (ASU)). Each *Pv*HPPK–DHPS chain that was traced has 600 of 717 residues along with disordered and missing loops. The six molecules of HPPK–DHPS in the ASU are designated A to F that form three biological dimers called AB, CD, and EF. The three dimers are similar, and their root mean squared deviations (RMSDs) for Cα atoms are generally <0.5 Å; they differ mostly in their long flexible loop regions. The N-terminal 10 residues and loop residues 55–80, 145–160, 189–202, 320–435, and 588–660 are disordered in all six molecules of HPPK–DHPS. The overall fold of the *Pv*HPPK–DHPS domains is similar to their known homologs. The average B-factor for molecules A, C, and D is ~37 Å^2, whereas for the other three molecules B, E, and F it is ~51Å^2. Therefore, from hereon the structural analyses discussed are based on the CD dimer (Fig. 2*A*). The RMSD between the *Pv*HPPK–DHPS and known HPPK and DHPS structures is <1 Å for the overlapping ferredoxin fold (C^α atoms 65–95) and the triosephosphate isomerase TIM barrel core (C^α atoms 165–195). The *Pv*HPPK–DHPS was crystallized in the presence of 6-hydroxymethylpterin-diphosphate (PtPP), pterin, the ATP analog AMPCPP, and *p*ABA (Fig. 2*A*). The electron densities for bound ligands are clear for the monomeric chains of *Pv*HPPK–DHPS (Fig. 2, *B* and *C*). The electron densities for whole AMPCPP or terminal phosphate groups of the AMPCPP are weak in monomers B, D, E, and F, possibly because of their poor occupancies. The present crystal structure therefore represents a holo form of the *Pv*HPPK–DHPS enzyme and will be discussed below in this light.

*Pv*HPPK has a 90-residue insertion (residues 60–150) between β-strands 2 and 3 when compared with the known homologs of HPPK structures from *Escherichia coli*, *Streptococcus pneumoniae*, *Yersinia pestis* (*Yp*), *Saccharomyces cerevisiae*, and *Francisella tularensis* (Figs. 3 and 4*A*) (23–28). This insertion wraps around the ferredoxin fold of *Pv*HPPK domain, and it has three α-helices: α1′a, α1′b, and α1′c. α1′a partially masks the active site of *Pv*HPPK (Fig. 4*A*). The loop (L3) between β-strands β5 and β6 are important for ATP binding in HPPK (Fig. 4*A*). In *Pv*HPPK, a 48-residue-long insertion (residues 222–260) is present in ATP-binding loop, and this insert has two α-helices (α2′a and α2′b) when compared with the known HPPK structures (Fig. 4*A*).

Clear electron densities in *Pv*DHPS are evident for *p*ABA and the substrate analog PtPP (Fig. 2*C*). In addition, well defined electron densities were observed for all the active-site loops in *Pv*DHPS because they are highly ordered (Fig. 4*B*). Long insertions are not found in the core-TIM barrel fold of *Pv*DHPS domain. However, a 40-residue insertion is present between strand β3 and helix α2, and this insertion has a 10-residue helix α2′ (Fig. 4*B*). The helix α2 of *Pv*DHPS has 26 residues in 7 turns and is up to 9 residues longer than the other known DHPS structures that have between 14 and 17 residues (Fig. 4*B*) (23–28). A Mg^{2+} cofactor is known to coordinate the diphosphate group within DHPPP and involves the conserved Asn^{342} in *Pv*HPPK–DHPS. In *Pv*DHPS, another 80-residue-long insertion is present between α-helix 7′ and α7, and this insertion contains the 8× "tandem repeat-like" sequence motif of GEGKLTN (Fig. 4*B*).

*Pv*HPPK–DHPS forms a dimeric assembly via C-terminal α-helices α6, α7′, α7, and α8 (Fig. 4*C*). In its dimeric form, the solvent-accessible surface of *Pv*HPPK–DHPS is ∼51,800 $Å^2$, and the buried surface is ∼3300 $Å^2$. The association of helices α6, α7′, α7, and α8 is similar to that observed in all dimeric DHPS structures, as also in the bifunctional *Sc*HPPK–DHPS structure (23–28). The dimer interface involves only the DHPS domain structural elements. In *Pv*DHPS, the N-terminal end of the TIM barrel is capped by antiparallel β-strands, and they are conserved among *E. coli* and *Yp*), *Thermus thermophilus* and *Bacillus anthracis* DHPSs (23–28). The capped anti-parallel β-sheet serves as a linker region between *Pv*HPPK and *Pv*DHPS domains. The linker β-strand (L1) forms a short antiparallel association with the β2-strand of *Pv*HPPK domain (Figs. 3 and 4*D*). This is very similar to *Sc*HPPK–DHPS structure (25). The orientation of HPPK domains does not overlap on the *F. tularensis* HPPK–DHPS (*Ft*HPPK–DHPS) structure (27), and large displacement in HPPK is observed in context of *Sc*HPPK–DHPS (Fig. 4*D*) (25). This is due to the longer β-strands in linker region of *Sc*HPPK–DHPS and shorter linker in *Ft*HPPK–DHPS when compared with the *Pv*HPPK–DHPS.

The molecular mechanism of sulfadoxine resistance

Our crystal structure of *Pv*DHPS in complex with *p*ABA shows a striking state of enzymatic activation in which five *Pv*DHPS loops bind *p*ABA onto the protein surface (Fig. 5*A*). The substrate *p*ABA is ensconced by loops 1, 2, 5, and 6 and the 7′ helix within loop 7. The eight key residues envelope *p*ABA in *Pv*DHPS and thus form its binding site that contains Phe^{348}, Ser^{382}, Ala^{383}, Pro^{384}, Gly^{551}, Phe^{552}, Lys^{581}, and Arg^{582} (Fig. 5*B*). These residues are highly conserved among *Pv* and *Pf*HPPK–DHPSs (Fig. 3, highlighted in the *box*). In addition to the *Pv*DHPS crystal structure reported here, the crystal structure of *Yp*DHPS bound to *p*ABA is known (28). Therefore, we compared the *p*ABA-binding residues and their conformational states in *Pv*DHPS and *Yp*DHPS. Loops 1 and 2 encapsulating *p*ABA in *Pv* and *Yp* are shown in (Fig. 5*C*), and they show no significant differences. In *Pv*DHPS, key residues caging *p*ABA in loop 2 are ^{381}SSAPY^{385}, whereas in *Yp* the residues are ^{61}STRPG^{65} (Fig. 5, *C* and *D*). Among these, it is evident that the proline in fourth position is conserved; it nestles the benzene ring of *p*ABA via a hydrophobic interaction (Figs. 5*D* and 6*C*). The two flexible loops 1 and 2 that cover *p*ABA-binding site are highly ordered in the present *Pv*HPPK–DHPS. In case of bacterial DHPS, the majority of the mutations known to confer resistance to sulfonamides are found in these two loops. However, in the case of *Pv*HPPK–DHPS, SDX point mutations do not occur in loop 1 that contributes the single *p*ABA-binding residue Phe^{348}.

The *p*ABA-binding residues Phe^{348}, Gly^{551}, Phe^{552}, Ser^{382}, Ala^{383}, Lys^{581}, Arg^{582}, and Pro^{384}, as well as the SDX resistance mutations are conserved among human malaria parasites *Pv* and *Pf* (Fig. 6*A*). Five SDX point mutations at positions S382F/A/C, A383G, K512E/M/T, A553G, and V585A have been reported in *Pv*DHPS (29–34) (Fig. 6*B*). These amino acid changes occur as singles (V585A or A383G), in doubles (A383G and A553G), or triply (S382A, A383G and A553G) and together account for DHPS mutations in 90% of the clinical isolates from malaria endemic regions (29–34). Our *Pv*HPPK–DHPS crystal structure shows that these resistance mutations surrounding the *p*ABA-binding site are present within loop 2 (S382/F/A/C and A383G), loop 5 (Lys^{512}), loop 6 (Ala^{553}), and 7′ helix in loop 7 (Val^{585}) (Figs. 3 and 6*B*).

We collated SDX resistance data from clinical isolates of *Pf* and *Pv* and analyzed available enzyme kinetic data from two elegant published studies in context of *p*ABA and SDX affinities (33, 34). We assessed the fold difference of the substrate-binding constant (K_m) of *p*ABA with the inhibitory constant (K_i) of SDX as a function of the DHPS mutations from both studies (33, 34) (Fig. 6*A*). It is documented that single amino acid mutations of A383G and V585A do not seem to confer very high levels of SDX resistance, as shown in Fig. 6*A* (33, 34). We also observed that the five key mutations responsible for SDX drug resistance mostly precede or succeed the vital atomic interactions that fall within 4 Å of the *p*ABA binding pocket (Fig. 6*B*). The residues Ser^{382} and Ala^{383} are present within loop 2 of *Pv*DHPS, and from analyses of deposited DHPS structures, it is evident that loop 2 is highly flexible and that its sequence is conserved across DHPSs. Further, in the case of *Pv*DHPS, loop 2 clearly stabilizes *p*ABA binding by contributing (Ser^{382}, Ala^{383}, and Pro^{384}) residues for *p*ABA recognition. Based on analysis of our *Pv*HPPK–DHPS crystal structure, it is evident that Ser^{382} and Ala^{383} residues make intimate interactions with *p*ABA (Fig. 5*B*). Further, Ser^{382} and Ala^{383} precede the critical Pro^{384} residue that stacks with the benzene ring of *p*ABA (Figs. 5*D* and 6*C*). These structural constraints within the *p*ABA-binding site likely explain the mutational effects of residues 382

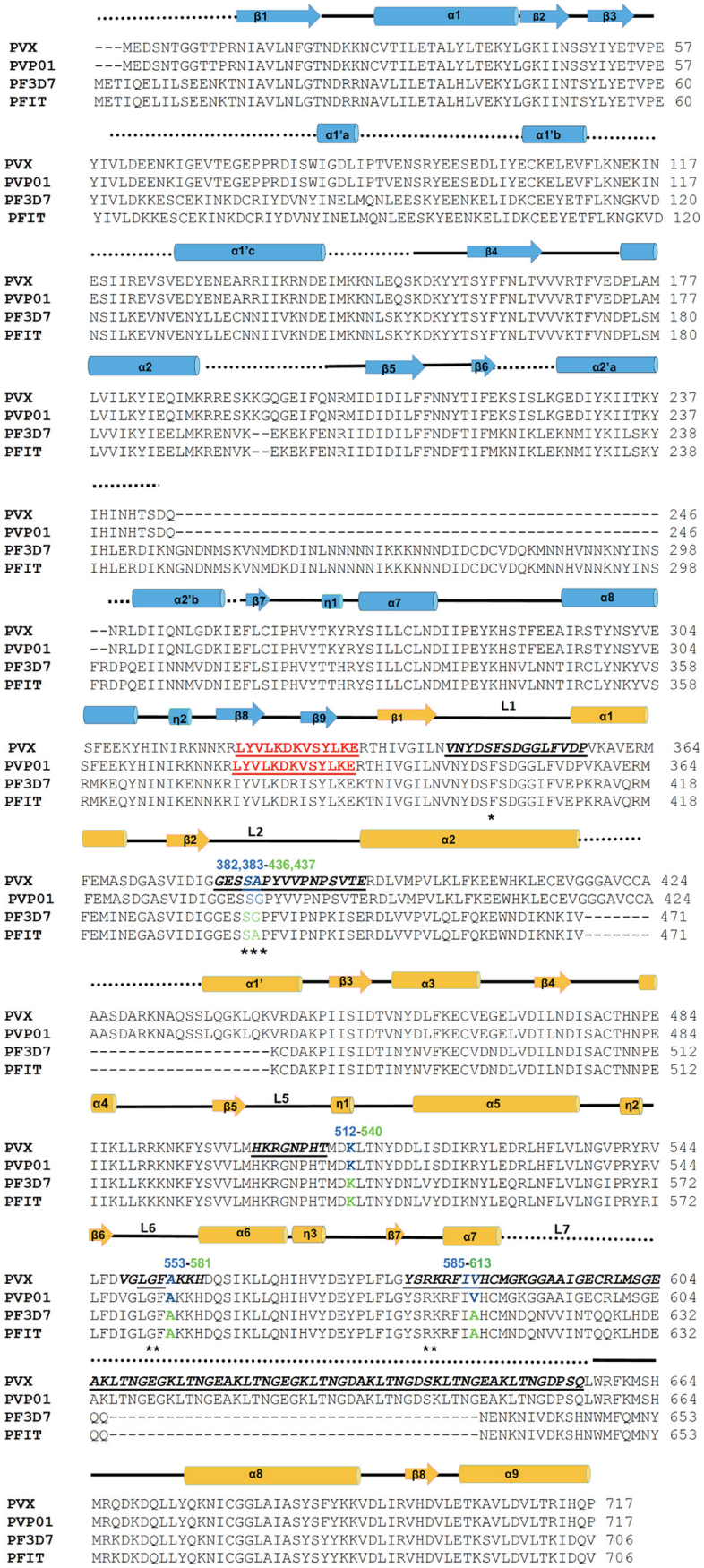
β1 α1 β2 β3
PVX ---MEDSNTGGTTPRNIAVLNFGTNDKKNCVTILETALYLTEKYLGKIINSSYIYETVPE 57
PVP01 ---MEDSNTGGTTPRNIAVLNFGTNDKKNCVTILETALYLTEKYLGKIINSSYIYETVPE 57
PF3D7 METIQELILSEENKTNIAVLNLGTNDRRNAVLILETALHLVEKYLGKIINTSYLYETVPE 60
PFIT METIQELILSEENKTNIAVLNLGTNDRRNAVLILETALHLVEKYLGKIINTSYLYETVPE 60
α1'a α1'b
PVX YIVLDEENKIGEVTEGEPPRDISWIGDLIPTVENSRYEESEDLIYECKELEVFLKNEKIN 117
PVP01 YIVLDEENKIGEVTEGEPPRDISWIGDLIPTVENSRYEESEDLIYECKELEVFLKNEKIN 117
PF3D7 YIVLDKKESCEKINKDCRIYDVNYINELMQNLEESKYEENKELIDKCEEYETFLKNGKVD 120
PFIT YIVLDKKESCEKINKDCRIYDVNYINELMQNLEESKYEENKELIDKCEEYETFLKNGKVD 120
α1'c β4
PVX ESIIREVSVEDYENEARRIIKRNDEIMKKNLEQSKDKYYTSYFFNLTVVVRTFVEDPLAM 177
PVP01 ESIIREVSVEDYENEARRIIKRNDEIMKKNLEQSKDKYYTSYFFNLTVVVRTFVEDPLAM 177
PF3D7 NSILKEVNVENYLLECNNIIVKNDEIMKNNLSKYKDKYYTSYFYNLTVVVKTFVNDPLSM 180
PFIT NSILKEVNVENYLLECNNIIVKNDEIMKNNLSKYKDKYYTSYFYNLTVVVKTFVNDPLSM 180
α2 β5 β6 α2'a
PVX LVILKYIEQIMKRRESKKGQGEIFQNRMIDIDILFFNNYTIFEKSISLKGEDIYKIITKY 237
PVP01 LVILKYIEQIMKRRESKKGQGEIFQNRMIDIDILFFNNYTIFEKSISLKGEDIYKIITKY 237
PF3D7 LVVIKYIEELMKRENVK--EKEKFENRIIDIDILFFNDFTIFMKNIKLEKNMIYKILSKY 238
PFIT LVVIKYIEELMKRENVK--EKEKFENRIIDIDILFFNDFTIFMKNIKLEKNMIYKILSKY 238
PVX IHINHTSDQ---------- 246
PVP01 IHINHTSDQ---------- 246
PF3D7 IHLERDIKNGNDNMSKVNMDKDINLNNNNNIKKKNNNDIDCDCVDQKMNNHVNNKNYINS 298
PFIT IHLERDIKNGNDNMSKVNMDKDINLNNNNNIKKKNNNDIDCDCVDQKMNNHVNNKNYINS 298
α2'b β7 η1 α7 α8
PVX --NRLDIIQNLGDKIEFLCIPHVYTKYRYSILLCLNDIIPEYKHSTFEEAIRSTYNSYVE 304
PVP01 --NRLDIIQNLGDKIEFLCIPHVYTKYRYSILLCLNDIIPEYKHSTFEEAIRSTYNSYVE 304
PF3D7 FRDPQEIINNMVDNIEFLSIPHVYTTHRYSILLCLNDMIPEYKHNVLNNTIRCLYNKYVS 358
PFIT FRDPQEIINNMVDNIEFLSIPHVYTTHRYSILLCLNDMIPEYKHNVLNNTIRCLYNKYVS 358
η2 β8 β9 β1 L1 α1
PVX SFEEKYHINIRKNNKRLYVLKDKVSYLKERTHIVGILNVNYDSFSDGGLFVDPVKAVERM 364
PVP01 SFEEKYHINIRKNNKRLYVLKDKVSYLKERTHIVGILNVNYDSFSDGGLFVDPVKAVERM 364
PF3D7 RMKEQYNINIKENNKRIYVLKDRISYLKEKTNIVGILNVNYDSFSDGGIFVEPKRAVQRM 418
PFIT RMKEQYNINIKENNKRIYVLKDRISYLKEKTNIVGILNVNYDSFSDGGIFVEPKRAVQRM 418
β2 L2 α2
382,383-436,437
PVX FEMASDGASVIDIGGESSAPYVVPNPSVTERDLVMPVLKLFKEEWHKLECEVGGGAVCCA 424
PVP01 FEMASDGASVIDIGGESSGPYVVPNPSVTERDLVMPVLKLFKEEWHKLECEVGGGAVCCA 424
PF3D7 FEMINEGASVIDIGGESSGPFVIPNPKISERDLVVPVLQLFQKEWNDIKNKIV------- 471
PFIT FEMINEGASVIDIGGESSAPFVIPNPKISERDLVVPVLQLFQKEWNDIKNKIV------- 471
α1' β3 α3 β4
PVX AASDARKNAQSSLQGKLQKVRDAKPIISIDTVNYDLFKECVEGELVDILNDISACTHNPE 484
PVP01 AASDARKNAQSSLQGKLQKVRDAKPIISIDTVNYDLFKECVEGELVDILNDISACTHNPE 484
PF3D7 ----------KCDAKPIISIDTINYNVFKECVDNDLVDILNDISACTNNPE 512
PFIT ----------KCDAKPIISIDTINYNVFKECVDNDLVDILNDISACTNNPE 512
α4 β5 L5 η1 α5 η2
512-540
PVX IIKLLRRKNKFYSVVLMHKRGNPHTMDKLTNYDDLISDIKRYLEDRLHFLVLNGVPRYRV 544
PVP01 IIKLLRRKNKFYSVVLMHKRGNPHTMDKLTNYDDLISDIKRYLEDRLHFLVLNGVPRYRV 544
PF3D7 IIKLLKKKNKFYSVVLMHKRGNPHTMDKLTNYDNLVYDIKNYLEQRLNFLVLNGIPRYRI 572
PFIT IIKLLKKKNKFYSVVLMHKRGNPHTMDKLTNYDNLVYDIKNYLEQRLNFLVLNGIPRYRI 572
β6 L6 α6 η3 β7 α7 L7
553-581 585-613
PVX LFDVGLGFAKKHDQSIKLLQHIHVYDEYPLFLGYSRKRFIVHCMGKGGAAIGECRLMSGE 604
PVP01 LFDVGLGFAKKHDQSIKLLQHIHVYDEYPLFLGYSRKRFIVHCMGKGGAAIGECRLMSGE 604
PF3D7 LFDIGLGFAKKHDQSIKLLQNIHVYDEYPLFIGYSRKRFIAHCMNDQNVVINTQQKLHDE 632
PFIT LFDIGLGFAKKHDQSIKLLQNIHVYDEYPLFIGYSRKRFIAHCMNDQNVVINTQQKLHDE 632
PVX AKLTNGEGKLTNGEAKLTNGEGKLTNGDAKLTNGDSKLTNGEAKLTNGDPSQLWRFKMSH 664
PVP01 AKLTNGEGKLTNGEAKLTNGEGKLTNGDAKLTNGDSKLTNGEAKLTNGDPSQLWRFKMSH 664
PF3D7 QQ----------NENKNIVDKSHNWMFQMNY 653
PFIT QQ----------NENKNIVDKSHNWMFQMNY 653
α8 β8 α9
PVX MRQDKDQLLYQKNICGGLAIASYSFYKKVDLIRVHDVLETKAVLDVLTRIHQP 717
PVP01 MRQDKDQLLYQKNICGGLAIASYSFYKKVDLIRVHDVLETKAVLDVLTRIHQP 717
PF3D7 MRKDKDQLLYQKNICGGLAIASYSYYKKVDLIRVHDVLETKSVLDVLTKIDQV 706
PFIT MRKDKDQLLYQKNICGGLAIASYSYYKKVDLIRVHDVLETKSVLDVLTKIDQV 706

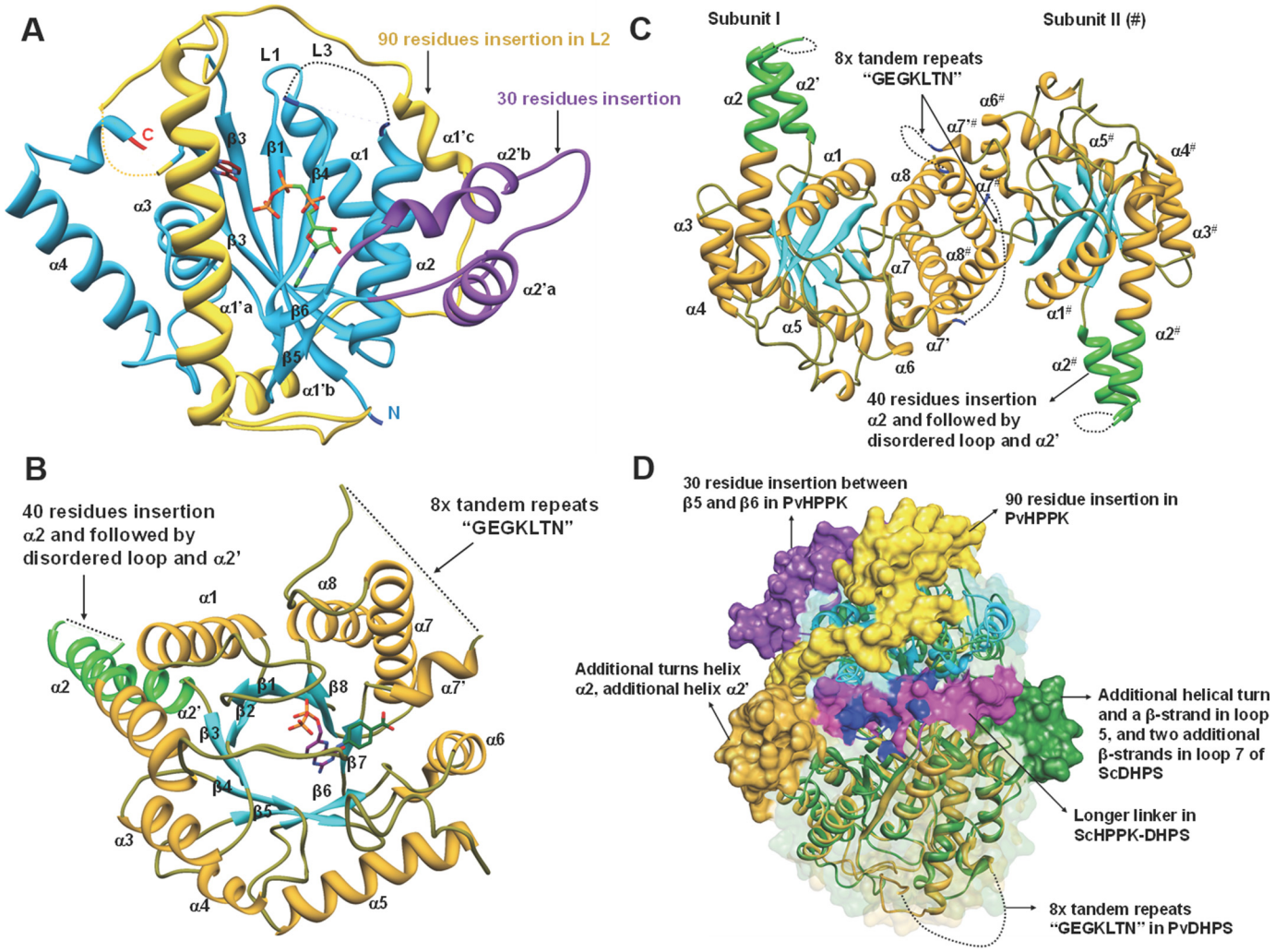

Figure 4. PvHPPK–DHPS domains and structural comparisons. *A* and *B*, the domains of *Pv*HPPK–DHPS are shown with secondary structural elements. The unique features/larger insertions are also labeled. *C*, a view of dimer interface and the participating helices α6, α7′, α7, and α8. A possible tandem repeat motif is shown. *D*, the superposition of DHPS domain of *Pv*HPPK–DHPS on *Sc*HPPK–DHPS where their unique features are highlighted.

and 383, because their mutation may disturb the positioning of Pro^{384} that is critical for stacking with the benzene ring of *p*ABA. Intriguingly, resistance mutation residue Lys^{512} lies distal to the *p*ABA-binding site, and its role in resistance generation cannot be reliably accessed via the present HPPK–DHPS structure (Fig. 6*B*). The A553G mutation will likely create alteration in the presentation of loop 6 that interacts with *p*ABA. The SDX mutant residue V585A shows a 2-fold increase in the level of resistance compared with the WT *Pv*DHPS (Fig. 6*A*); this residue is located at dimerization interface and does not seem to play a role in the binding of either the substrate or SDX (not shown). Interestingly, our *Pv*HPPK–DHPS structure reveals that residues Arg^{582} and Asp^{511} make salt-bridge interactions and are conserved in *Pv* and *Pf* HPPK–DHPSs. It is likely that the V585A mutation results in steric hindrance with Arg^{582}. This may translate into diminished interactions with Asp^{511} and structural perturbation of *p*ABA recognition (Fig. 6*C*).

Discussion

The X-ray structure of *Pv*HPPK–DHPS presented here rationalizes the known sulfa drug resistance mutations that have arisen over the past four decades as a result of drug usage. The *Pv*HPPK–DHPS structural analyses reveal an intricate dimeric assembly via a C-terminal region in the *Pv*DHPS sequence. This long-awaited crystal structure of the malaria parasite's unique bifunctional HPPK–DHPS enzyme reveals the exquisite structural subtleties involved in SDX resistance generation. It is evident that most SDX resistance mutations map proximal to the *p*ABA-binding site, where they are likely to subtly alter the intricate atomic interactions such that enzyme affinity for *p*ABA is only diminished moderately (up to 11-fold), but K_i for

Figure 3. Structure-based sequence alignment of malaria parasite HPPK–DHPSs. The secondary structure elements of *Pv*HPPK–DHPS (*blue*) and *Pf*HPPK–DHPS (*yellow*) are marked, with α- and 3_{10}-helices (*cylinders*) and β-strands (*arrows*). The *p*ABA-binding loops (L1, L2, L5, L6, and L7) residues are in *bold*, *underlined*, and labeled. The disordered regions in the crystal structure of *Pv*HPPK–DHPS are marked by *black dots*. The SDX resistance mutations in *Pf* (*green*) and *Pv* (*blue*) are numbered above the sequences. The linker region between HPPK and DHPS is highlighted in *red*. The *p*ABA-binding residues are marked with *stars*.

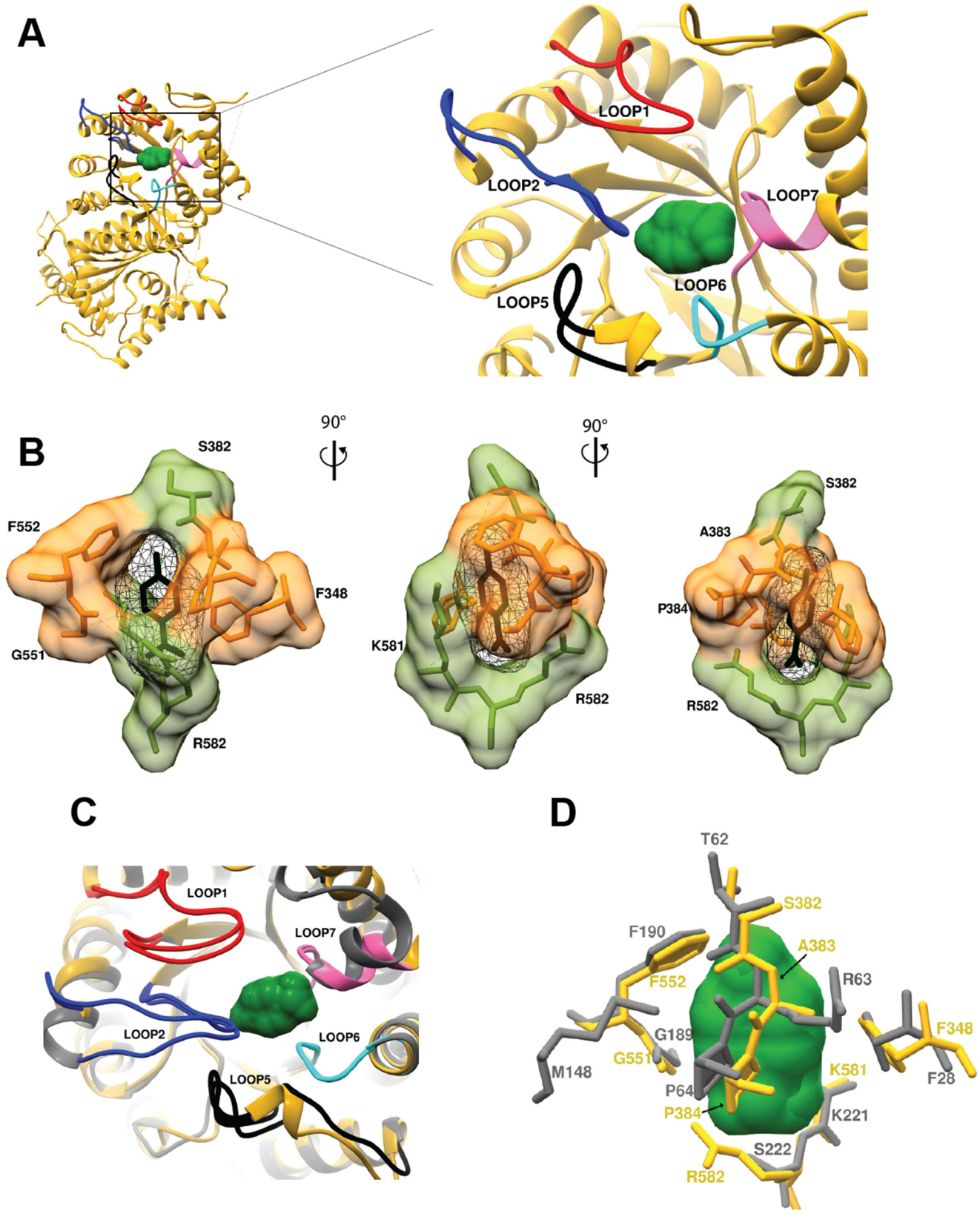

Figure 5. The *p*ABA-binding site in *Pv*DHPS. *A*, overall view of the *p*ABA-binding region with key loops labeled. *B*, key residues that cage *p*ABA in *Pv*DHPS. *C*, structural comparisons between loops that surround *p*ABA in DHPSs from *Y. pestis* and *P. vivax*. *D*, critical *p*ABA-binding residues in *Pv* (*yellow*) and *Yp* (*gray*) are shown. The *p*ABA molecule is shown as molecular surface (*green*) and protein residues shown as sticks (*gray* and *yellow*).

A

	382	383	512	553	585
Pv DHPS	S	A	K	A	V
Pf DHPS	S	A	K	A	A
	436	437	540	581	612

Pv DHPS mutations	A383G	V585A	A383G, A553G	S382A, A383G, A553G
Δfold *p*ABA/SDX Km/Ki	2/32	1/2	3/117	1/177
Pf DHPS mutations	S436A/S/F, A437G	A437G, A581G	S436A/S/F, A437G, K540E/N	S436A/S/F, A437G, A581G
Δfold *p*ABA/SDX Km/Ki	5/142	4/115	6/702	11/805

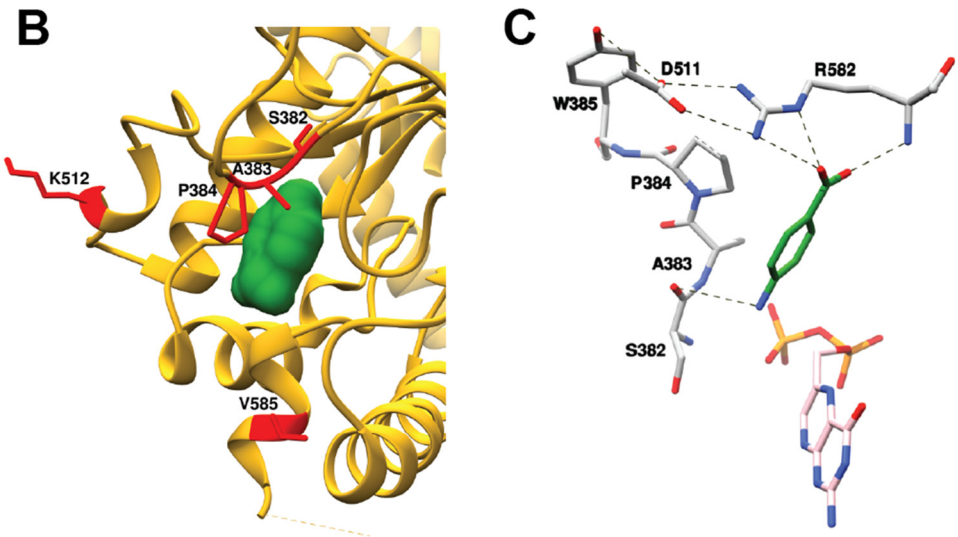

Figure 6. Enzymatic data. *A*, the kinetic parameters K_m and K_i values for SDX resistance mutations in *Pf* and *Pv* based on previous studies (33, 34). The fold change in substrate affinity and drug potency were calculated using published data (41, 42). *B*, the *p*ABA-bound *Pv*DHPS domain with the mutant residues is highlighted in *red*. *C*, the important salt-bridge interactions between Arg^{582} and Asp^{511} are shown with *dotted lines* along with hydrogen-bonding networks around *p*ABA binding site in *Pv*DHPS.

SDX is altered substantially (more than 100-fold for double/triple mutants in both *Pv*/*Pf* DHPSs (Fig. 6*A*). Thus, a structural compromise is reached in the drug resistant enzyme wherein marginal lowering in the substrate (*p*ABA) affinity (K_m = ~11-fold) is traded for substantial reductions (K_i = ~800-fold; Fig. 6*A*) in SDX drug potency. This trick, although highly successful, also opens the enzyme for targeting via novel inhibitors that are designed based on the exact substrate envelope such that new inhibitors fit and colonize the substrate-binding site fully and that too in at least four different druggable pockets that are evident in the *Pv*HPPK–DHPS structure. Indeed, inhibitors like SDX that protrude beyond the substrate envelope may encourage development of mutations that confer drug resistance. In this light, an interesting drug design approach has been applied toward potentially overcoming drug resistance in HIV by focusing on inhibitors that fit snugly in the small substrate-binding cavity of HIV protease (35, 36).

It is noteworthy that the *Pv*HPPK–DHPS residues involved in recognition of pterin moiety in both domains are highly conserved. This presents yet another opportunity to target conserved motifs within *Pv*HPPK–DHPS now that the crystal structure is available (37). The presented *Pv*HPPK–DHPS structure indicates that sulfa-drug resistance mutations emanate from a structural compromise in the mutant drug resistance enzyme that enables rejection of the drug while minimally altering affinity for its substrate *p*ABA. Although our *p*ABA-bound *Pv*HPPK–DHPS crystal structure can explain SDX resistance for most mutations, we feel that SDX-bound crystal structures of mutant and WT *Pv*DHPSs are required for a deeper understanding of this enzyme/drug system (37). From our structural analysis of *Pv*HPPK–DHPS and its mutations in context of sulfadoxine resistance, we have generated several insights including (*a*) the presented structure should be exploited to identify nonsulfa drugs that do not mimic *p*ABA and thus inhibit the enzyme irreversibly, (*b*) the *Plasmodium* HPPK domain can now be utilized for focusing on pterin-based inhibitors (38), (*c*) designing drugs that target the triple mutant in *Pv*HPPK–DHPS will be valuable because they can be selectively administered in regions of prevalent SDX resistance, and (*d*) twin targeting of *Plasmodium* HPPK and the DHPS subdomains within *Pv*HPPK–DHPS may provide more potent inhibition of the enzyme. This work therefore provides excep-

tional opportunities to exploit the structure of *Pv*HPPK–DHPS for screening of drug-like libraries to identify drug scaffolds that can occupy any one or more of its substrate pockets in addition to the *p*ABA-binding site.

Experimental procedures

Gene cloning and protein production

Full-length *Pv*HPPK–DHPS (1–717 amino acids) was purchased as a gBlock (Integrated DNA Technologies, Leuven, Belgium). The ORF of full-length *Pv*HPPK–DHPS (residues 1–717) was optimized for expression in the *E. coli* strain Rosetta-pLysS and cloned into the pOPINF vector that was linearized using NcoI and SalI restriction sites. Transformed *E. coli* strain Rosetta-pLysS was grown in LB medium containing 100 μg ml^{-1} ampicillin and 34 μg ml^{-1} chloramphenicol to an A_{600} of 0.6–0.8 at 37 °C. Expression of the His_6-tagged recombinant *Pv*HPPK–DHPS was induced by the addition of 0.5 mM isopropyl β-D-galactoside, and culture was further incubated at 18 °C for 20 h. Bacterial cells were lysed by a combination of lysozyme treatment and sonication in buffer with 50 mM Tris, pH 8, 500 mM NaCl, 10% glycerol, 10 mM imidazole, 1 mM phenylmethylsulfonyl fluoride, and 1 mM benzamidine HCl. Recombinant protein was affinity captured using nickel–nitrilotriacetic acid–agarose beads (Qiagen) followed by cleavage at 20 °C with 3C-protease for removal of the His_6 tag. Protein was subsequently applied to Q-Sepharose (GE Healthcare) column in buffer with 50 mM Tris, pH 8.0, 250 mM NaCl, 5 mM β-mercaptoethanol. Protein from the flow through fraction was then processed using hydrophobic interaction chromatography on a Phenyl FF 16/10 column (GE Healthcare). Pure fractions obtained from hydrophobic interaction chromatography were pooled and concentrated with 30-kDa cutoff centrifugal devices (Millipore) followed by gel permeation chromatography on a S-200–16/60 column (GE Healthcare) in a buffer containing 50 mM HEPES, pH 6.8, 200 mM NaCl, 5 mM β-mercaptoethanol. A single peak corresponding to dimeric *Pv*HPPK–DHPS was collected from gel permeation chromatography.

Crystallization and data collection

The purified full-length *Pv*HPPK–DHPS (~10 mg ml^{-1}) was used for crystallization screening in the presence of PtPP (0.5 mM), pterin (0.5 mM), AMPCPP (1 mM), and *p*ABA (3 mM) using the hanging-drop vapor-diffusion method at 20 °C with commercially available crystallization screens (Hampton and Molecular Dimensions). The initial screening was carried out in 96-well plates using nano-drop dispensing mosquito robot (TTP Lab Tech). Diffraction quality crystals were obtained using 20% PEG 3350, 0.2 M potassium citrate tribasic monohydrate as mother liquor. The crystals were harvested using corresponding crystallization solution supplemented with 20% (v/v) ethylene glycol as a cryo-protectant and were flash-frozen into liquid nitrogen. Preliminary data collection screening was conducted at PROXIMA 1 Beamline (Soleil, France), and a high-resolution data set was collected at 100 K using Pilatus3 6 M detector (Dectris) and wavelength (λ) of 0.9763 Å at I03 Beamline, Diamond Light Source in the United Kingdom. The data were processed and scaled with XIA2 (39) using DIALS (40), and data processing statistics are shown in Table 1.

Table 1
X-ray data collection and refinement statistics
The numbers in the parentheses are for the highest resolution bin.

Source	I03, DLS
Data collection	
Wavelength (Å)	0.9763
Oscillation width (°)	0.1
Exposure time (s)	0.02
Cell parameters (Å, °)	136.05, 113.89, 172.39; 94.24
Space group	P 2_1
Resolution	113.89–2.79 (2.79–2.84)
Number of unique reflections	129475 (5799)
$I/\sigma(I)$	4.5 (0.7)
$CC_{½}$	0.9 (0.2)
Completeness	99.4 (90.4)
Redundancy	3.5 (3.4)
Molecules/ASU	6
Solvent content (%)	56
Matthews coefficient V_m (Å Da^{-1})	2.75
Refinement	
Refinement resolution (Å)	50.0–2.90 (2.95–2.90)
Reflections used in refinement	114185
Reflections in working set	112179 (8347)
Test set	2006 (144)
R_{factor}/R_{free} (%)	24.2/28.5
Number of atoms	
Protein	28365
Ligands	342
Water	217
B-factors (Å^2)	
Protein	43.8
Ligands	46.3
Waters	18.2
Ramachandran plot (%)	
Favored regions	94
Allowed regions	6
RMSD	
Bond lengths (Å)	0.014
Bond angles (°)	1.643

Structure determination

Preliminary X-ray data analysis indicated that the *Pv*HPPK–DHPS crystals contain ~56% solvent with Matthews coefficient of 2.75 Å^3 Da^{-1} for six full-length *Pv*HPPK–DHPS protomers in the ASU. Attempts to solve the phase problem using molecular replacement (MR) techniques with PHASER (41) as implemented in PHENIX (42) and coordinates of fused bifunctional HPPK–DHPS enzyme of *S. cerevisiae* (*Sc*HPPK–DHPS; PDB code 2BMB) and *F. tularensis* (*Ft*HPPK–DHPS; PDB code 4PZV) as template were unsuccessful. In both *Sc*HPPK–DHPS and *Ft*HPPK–DHPS, the orientation of the HPPK domains did not overlap while superposing the DHPS domains. Therefore, the available dimeric DHPS domain structures were fed as template, and most of the MR runs placed three dimers with log-likelihood gain value in the range of 300–600 and with translation function *Z* score of 5.5–6.8. The R_{free} for these models were >50% for most of the templates except with *Mycobacterium tuberculosis* dimeric DHPS (PDB code 1EYE) model (43), which gave a starting R_{free} of 49%. The initial $F_o - F_c$ map revealed significant unbiased regions of positive connected electron density that did not form part of the DHPS probe; this thus indicated a correct MR solution. The initial atomic model was subjected to AutoBuild in PHENIX (42) that provided a partial model with R_{free} of 46% for ~1500 residues in several chains with three dimeric cores of DHPS. Subsequently, the model was manually built, extended and completed by several

cycles of iterative building using COOT (44) and REFMAC (45). Map interpretation and model building was based on electron densities in difference Fourier ($F_o - F_c$), $2F_o - F_c$ and composite omit maps. In all stages, model building was guided by manual inspection of the model and R_{free}. The substrate/analogs and water molecules were added into the difference Fourier maps ($F_o - F_c$). The modeled ligands and protein residues were validated using simulated annealing composite omit maps. The occupancies of the ligand molecules were refined and weakly bound ligands, highly disordered loops (residues numbered 1–10, 55–80, 189–202, and 420–434) and low complexity regions (residues 588–660) were not included in the final model. The final refinement statistics are shown in Table 1. The coordinates and structure factors for *Pv*HPPK–DHPS have been deposited in the PDB under accession code 5Z79. The figures were generated using CHIMERA (46) and PyMOL (47).

Author contributions—M. Y. and Am. S. were responsible for conceptualization, formal analysis, supervision, funding acquisition, and investigation; M. Y. and Am. S. solved the structure of *Pv*HPPK–DHPS; J. E. N. and K. H. provided the recombinant clones; K. H. collected diffraction data.; Ak.S. and A.J. performed expression, purification, and crystallization using a construct screened and developed by J. E. N; R. C., M. S., and J. C. G. maintained the clones; M. Y., Am. S., and J. C. G. analyzed the data and wrote the manuscript.

Acknowledgments—We thank the beam line staff at PROXIMA 1 and PROXIMA 2A for assistance during data collection at SOLEIL. We also thank staff at Diamond for access to Beamline I03 (MX14744).

References

1. World Health Organization (2017) World Malaria Report, World Health Organization, Geneva, Switzerland
2. Fidock, D. A., Eastman, R. T., Ward, S. A., and Meshnick, S. R. (2008) Recent highlights in antimalarial drug resistance and chemotherapy research. *Trends Parasitol.* **24,** 537–544 CrossRef Medline
3. Fidock, D. A. (2010) Drug discovery: priming the antimalarial pipeline. *Nature* **465,** 297–298 CrossRef Medline
4. Ragsdale, S. W. (2008) Catalysis of methyl group transfers involving tetrahydrofolate and B12. *Vitam. Horm.* **79,** 293–324 CrossRef Medline
5. Müller, I. B., and Hyde, J. E. (2013) Folate metabolism in human malaria parasites: 75 years on. *Mol. Biochem. Parasitol.* **188,** 63–77 CrossRef Medline
6. Duffy, S., and Avery, V. M. (2013) Identification of inhibitors of *Plasmodium falciparum* gametocyte development. *Malar. J.* **12,** 408 CrossRef Medline
7. Nzila, A., Ward, S. A., Marsh, K., Sims, P. F., and Hyde, J. E. (2005) Comparative folate metabolism in humans and malaria parasites: I. pointers for malaria treatment from cancer chemotherapy. *Trends Parasitol.* **21,** 292–298 CrossRef Medline
8. Shiota, T. (1984) Biosynthesis of folate from pterin precursors. In *Chemistry and Biochemistry of Folates* (Blakley, R., and Benkovic, S., eds) pp. 121–134, John Wiley & Sons, New York
9. Blaszczyk, J., Shi, G., Li, Y., Yan, H., and Ji, X. (2004) Reaction trajectory of pyrophosphoryl transfer catalyzed by 6-hydroxymethyl-7,8-dihydropterin pyrophosphokinase. *Structure* **12,** 467–475 CrossRef Medline
10. Chotpatiwetchkul, W., Boonyarattanakalin, K., Gleeson, D., and Gleeson, M. P. (2017) Exploring the catalytic mechanism of dihydropteroate synthase: elucidating the differences between the substrate and inhibitor. *Org. Biomol. Chem.* **15,** 5593–5601 CrossRef Medline
11. Wright, D. L., and Anderson, A. C. (2011) Antifolate agents: a patent review (2006–2010). *Expert Opin. Ther. Pat.* **21,** 1293–1308 CrossRef Medline
12. Hammoudeh, D. I., Zhao, Y., White, S. W., and Lee, R. E. (2013) Replacing sulfa drugs with novel DHPS inhibitors. *Future Med. Chem.* **5,** 1331–1340 CrossRef Medline
13. Roland, S., Ferone, R., Harvey, R. J., Styles, V. L., and Morrison, R. W. (1979) The characteristics and significance of sulfonamides as substrates for *Escherichia coli* dihydropteroate synthase. *J. Biol. Chem.* **254,** 10337–10345 Medline
14. Achari, A., Somers, D. O., Champness, J. N., Bryant, P. K., Rosemond, J., and Stammers, D. K. (1997) Crystal structure of the anti-bacterial sulfonamide drug target dihydropteroate synthase. *Nat. Struct. Biol.* **4,** 490–497 CrossRef Medline
15. Gaudillière, J.-P. (2009) The first miracle drugs: how the sulfa drugs transformed medicine. *Bull. Hist. Med.* **83,** 218–220 CrossRef
16. Thaithong, S., Chan, S. W., Songsomboon, S., Wilairat, P., Seesod, N., Sueblinwong, T., Goman, M., Ridley, R., and Beale, G. (1992) Pyrimethamine resistant mutations in *Plasmodium falciparum*. *Mol. Biochem. Parasitol.* **52,** 149–157 CrossRef Medline
17. Pinichpongse, S., Doberstyn, E. B., Cullen, J. R., Yisunsri, L., Thongsombun, Y., and Thimasarn, K. (1982) An evaluation of five regimens for the outpatient therapy of *falciparum* malaria in Thailand 1980–81. *Bull. World Health Organ.* **60,** 907–912 Medline
18. Ferone, R. (1970) Dihydrofolate reductase from pyrimethamine-resistant *Plasmodium berghei*. *J. Biol. Chem.* **245,** 850–854 Medline
19. Chulay, J. D., Watkins, W. M., and Sixsmith, D. G. (1984) Synergistic antimalarial activity of pyrimethamine and sulfadoxine against *Plasmodium falciparum in vitro*. *Am. J. Trop. Med. Hyg.* **33,** 325–330 CrossRef Medline
20. Hurly, M. G. (1959) Potentiation of pyrimethamine by sulphadiazine in human malaria. *Trans. R. Soc. Trop. Med. Hyg.* **53,** 412–413 CrossRef Medline
21. World Health Organization (2010) WHO policy recommendation on intermittent preventive treatment during infancy for *Plasmodium falciparum* malaria control in Africa contra-indications, pp. 4–6, World Health Organization, Geneva, Switzerland
22. Conteh, L., Sicuri, E., Manzi, F., Hutton, G., Obonyo, B., Tediosi, F., Biao, P., Masika, P., Matovu, F., Otieno, P., Gosling, R. D., Hamel, M., Odhiambo, F. O., Grobusch, M. P., Kremsner, P. G., *et al.* (2010) The cost-effectiveness of intermittent preventive treatment for malaria in infants in sub-Saharan Africa. *PLoS One* **5,** e10313 CrossRef Medline
23. Blaszczyk, J., Li, Y., Cherry, S., Alexandratos, J., Wu, Y., Shaw, G., Tropea, J. E., Waugh, D. S., Yan, H., and Ji, X. (2007) Structure and activity of *Yersinia pestis* 6-hydroxymethyl-7,8-dihydropterin pyrophosphokinase as a novel target for the development of antiplague therapeutics. *Acta Crystallogr. D Biol. Crystallogr.* **63,** 1169–1177 CrossRef Medline
24. Garçon, A., Levy, C., and Derrick, J. P. (2006) Crystal structure of the bifunctional dihydroneopterin aldolase/6-hydroxymethyl-7,8-dihydropterin pyrophosphokinase from *Streptococcus pneumoniae*. *J. Mol. Biol.* **360,** 644–653 CrossRef Medline
25. Lawrence, M. C., Iliades, P., Fernley, R. T., Berglez, J., Pilling, P. A., and Macreadie, I. G. (2005) The three dimensional structure of the bifunctional 6-hydroxymethyl-7,8-dihydropterin pyrophosphokinase/dihydropteroate synthase of *Saccharomyces cerevisiae*. *J. Mol. Biol.* **348,** 655–670 CrossRef Medline
26. Chhabra, S., Dolezal, O., Collins, B. M., Newman, J., Simpson, J. S., Macreadie, I. G., Fernley, R., Peat, T. S., and Swarbrick, J. D. (2012) Structure of *S. aureus* HPPK and the discovery of a new substrate site inhibitor. *PLoS One* **7,** e29444 CrossRef Medline
27. Pemble, C. W., 4th, Mehta, P. K., Mehra, S., Li, Z., Nourse, A., Lee, R. E., and White, S. W. (2010) Crystal structure of the 6-hydroxymethyl-7,8-dihydropterin pyrophosphokinase·dihydropteroate synthase bifunctional enzyme from *Francisella tularensis*. *PLoS One* **5,** e14165 CrossRef Medline
28. Yun, M. K., Wu, Y., Li, Z., Zhao, Y., Waddell, M. B., Ferreira, A. M., Lee, R. E., Bashford, D., and White, S. W. (2012) Catalysis and sulfa drug resistance in dihydropteroate synthase. *Science* **335,** 1110–1114 CrossRef Medline

29. Snounou, G., and White, N. J. (2004) The co-existence of *Plasmodium*: sidelights from *falciparum* and *vivax* malaria in Thailand. *Trends Parasitol.* **20,** 333–339 CrossRef Medline
30. Auliff, A., Wilson, D. W., Russell, B., Gao, Q., Chen, N., Anh le, N., Maguire, J., Bell, D., O'Neil, M. T., and Cheng, Q. (2006) Amino acid mutations in *Plasmodium vivax* DHFR and DHPS from several geographical regions and susceptibility to antifolate drugs. *Am. J. Trop. Med. Hyg.* **75,** 617–621 Medline
31. Hawkins, V. N., Suzuki, S. M., Rungsihirunrat, K., Hapuarachchi, H. C., Maestre, A., Na-Bangchang, K., and Sibley, C. H. (2009) Assessment of the origins and spread of putative resistance-conferring mutations in *Plasmodium vivax* dihydropteroate synthase. *Am. J. Trop. Med. Hyg.* **81,** 348–355 Medline
32. Rungsihirunrat, K., Sibley, C. H., Mungthin, M., and Na-Bangchang, K. (2008) Geographical distribution of amino acid mutations in *Plasmodium vivax* DHFR and DHPS from malaria endemic areas of Thailand. *Am. J. Trop. Med. Hyg.* **78,** 462–467 Medline
33. Pornthanakasem, W., Riangrungroj, P., Chitnumsub, P., Ittarat, W., Kongkasuriyachai, D., Uthaipibull, C., Yuthavong, Y., and Leartsakulpanich, U. (2016) Role of *Plasmodium vivax* dihydropteroate synthase polymorphisms in sulfa drug resistance. *Antimicrob. Agents Chemother.* **60,** 4453–4463 CrossRef Medline
34. Triglia, T., Menting, J. G., Wilson, C., and Cowman, A. F. (1997) Mutations in dihydropteroate synthase are responsible for sulfone and sulfonamide resistance in *Plasmodium falciparum*. *Proc. Natl. Acad. Sci. U.S.A.* **94,** 13944–13949 CrossRef Medline
35. Nalam, M. N., Ali, A., Altman, M. D., Reddy, G. S., Chellappan, S., Kairys, V., Ozen, A., Cao, H., Gilson, M. K., Tidor, B., Rana, T. M., and Schiffer, C. A. (2010) Evaluating the substrate-envelope hypothesis: structural analysis of novel HIV-1 protease inhibitors designed to be robust against drug resistance. *J. Virol.* **84,** 5368–5378 CrossRef Medline
36. Altman, M. D., Ali, A., Reddy, G. S., Nalam, M. N., Anjum, S. G., Cao, H., Chellappan, S., Kairys, V., Fernandes, M. X., Gilson, M. K., Schiffer, C. A., Rana, T. M., and Tidor, B. (2008) HIV-1 protease inhibitors from inverse design in the substrate envelope exhibit subnanomolar binding to drug-resistant variants. *J. Am. Chem. Soc.* **130,** 6099–6113 CrossRef Medline
37. Bertacine Dias, M. V., Santos, J. C., Libreros-Zúñiga, G. A., Ribeiro, J. A., and Chavez-Pacheco, S. M. (2018) Folate biosynthesis pathway: mechanisms and insights into drug design for infectious diseases. *Future Med. Chem.* **10,** 935–959 CrossRef Medline
38. Yun, M. K., Hoagland, D., Kumar, G., Waddell, M. B., Rock, C. O., Lee, R. E., and White, S. W. (2014) The identification, analysis and structure-based development of novel inhibitors of 6-hydroxymethyl-7,8-dihydropterin pyrophosphokinase. *Bioorg. Med. Chem.* **22,** 2157–2165 CrossRef Medline
39. Winter, G., Lobley, C. M., and Prince, S. M. (2013) Decision making in xia2. *Acta Crystallogr. D Biol. Crystallogr.* **69,** 1260–1273 CrossRef Medline
40. Waterman, D. G., Winter, G., Gildea, R. J., Parkhurst, J. M., Brewster, A. S., Sauter, N. K., and Evans, G. (2016) Diffraction-geometry refinement in the DIALS framework. *Acta Crystallogr. D Struct. Biol.* **72,** 558–575 CrossRef Medline
41. McCoy, A. J., Grosse-Kunstleve, R. W., Adams, P. D., Winn, M. D., Storoni, L. C., and Read, R. J. (2007) Phaser crystallographic software. *J. Appl. Crystallogr.* **40,** 658–674 CrossRef Medline
42. Adams, P. D., Afonine, P. V., Bunkóczi, G., Chen, V. B., Davis, I. W., Echols, N., Headd, J. J., Hung, L. W., Kapral, G. J., Grosse-Kunstleve, R. W., McCoy, A. J., Moriarty, N. W., Oeffner, R., Read, R. J., and Richardson, D. C. (2000) PHENIX: A comprehensive Python-based system for macromolecular structure solution. *Acta Crystallogr. D Biol. Crystallogr.* **66,** 213–221.43
43. Baca, A. M., Sirawaraporn, R., Turley, S., Sirawaraporn, W., and Hol, W. G. (2000) Crystal structure of *Mycobacterium tuberculosis* 6-hydroxymethyl-7,8-dihydropteroate synthase in complex with pterin monophosphate: new insight into the enzymatic mechanism and sulfa-drug action. *J. Mol. Biol.* **302,** 1193–1212 CrossRef Medline
44. Emsley, P., Lohkamp, B., Scott, W. G., and Cowtan, K. (2010) Features and development of Coot. *Acta Crystallogr. D Biol. Crystallogr.* **66,** 486–501 CrossRef Medline
45. Murshudov, G. N., Skubák, P., Lebedev, A. A., Pannu, N. S., Steiner, R. A., Nicholls, R. A., Winn, M. D., Long, F., and Vagin, A. A. (2011) REFMAC 5 for the refinement of macromolecular crystal structures. *Acta Crystallogr. D Biol. Crystallogr.* **67,** 355–367 CrossRef Medline
46. Pettersen, E. F., Goddard, T. D., Huang, C. C., Couch, G. S., Greenblatt, D. M., Meng, E. C., and Ferrin, T. E. (2004) UCSF Chimera-a visualization system for exploratory research and analysis. *J. Comput. Chem.* **25,** 1605–1612 CrossRef Medline
47. DeLano, W. L. (2012) *The PyMOL Molecular Graphics System*, version 1.5.0.1, Schroedinger, LLC, New York